
THE EFFECT OF THE SEA-ICE ZONE ON THE DEVELOPMENT OF BOUNDARY-LAYER ROLL CLOUDS DURING COLD AIR OUTBREAKS

A. Q. LIU^{1,*}, G. W. K. MOORE¹, K. TSUBOKI² and I. A. RENFREW³

¹*Department of physics, University of Toronto, Toronto, Ontario Canada, M5S1A7;* ²*Nagoya University, Nagoya, Japan;* ³*University of East Anglia, Norwich, U.K.*

(Received in final form 15 April 2005 / Published online: 10 May 2006)

Abstract. High latitude air–sea interaction is an important component of the earth’s climate system and the exchanges of mass and energy over the sea-ice zone are complicated processes that, at present, are not well understood. In this paper, we perform a series of numerical experiments to examine the effect of sea-ice concentration on the development of high latitude boundary-layer roll clouds. The experiments are performed at sufficiently high spatial resolution to be able to resolve the individual convective roll clouds, and over a large enough domain to be able to examine the roll’s downstream development. Furthermore the high spatial resolution of the experiments allows for an explicit representation of heterogeneity within the sea-ice zone. The results show that the sea-ice zone has a significant impact on the atmospheric boundary-layer development, which can be seen in both the evolution of the cloud field and the development of heat and moisture transfer patterns. In particular, we find the air–sea exchanges of momentum, moisture and heat fluxes are modified by the presence of the roll vortices (typically a 10% difference in surface heat fluxes between up-drafts and downdrafts) and by the concentration and spatial distribution of the sea-ice. This suggests that a more realistic representation of processes over the sea-ice zone is needed to properly calculate the air–sea energy and mass exchange budgets.

Keywords: Air–sea interaction, Boundary layer, Cold air outbreaks, Numerical modelling, Roll clouds, Sea-ice zone.

1. Introduction

High-latitude air–sea interaction is an important component of the earth’s climate system. During wintertime cold air outbreaks, very cold and dry polar air flows over the relatively warm ocean resulting in the transfer of large amounts of heat, momentum and moisture between the ocean and atmosphere. Horizontal convective roll clouds, triggered by the development of Rayleigh–Benard convection, are often observed to be associated with this transfer. The modification of the atmosphere and ocean that

*E-mail: liugi@atmosph.physics.utoronto.ca

occurs as a result is important for the development of mesoscale cyclones and other forms of severe weather (Moore et al., 1996; Brummer, 1997; Rasmussen and Turner, 2003) as well as in oceanic processes such as deep ocean convection (Marshall et al., 1998; Renfrew et al., 1999).

Sea ice is a good insulator and so its presence typically reduces or eliminates this exchange thereby inhibiting the formation of convective clouds. However, heterogeneities in ice cover can allow for this transfer to take place *albeit* in a spatially complex manner (Renfrew et al., 1999; Pagowski and Moore, 2001). Satellite observations frequently capture convective roll clouds forming over the sea-ice zone, and their evolution into cellular convection with downstream distance from the ice edge. For example, in Figure 1 one can clearly see the complex spatially heterogeneous character of the sea-ice zone, as well as the formation of roll clouds over large leads and areas of open water. Model simulations indicate that variability in sea-ice concentration can have a significant impact on the global climate (Grotzner et al., 1996; Rind et al., 1997; Parkinson et al., 2001; Alexander et al., 2004).

Field observations have investigated the characteristics of boundary-layer roll clouds during cold air outbreaks in various locations, including the Beaufort Sea (Mourad and Walter, 1996a,b) the Bering Sea (Walter, 1980; Mourad and Walter, 1996a, b), the Greenland Sea (Brummer et al., 1992, 1994; Brummer and Thiemann, 2002), the Labrador Sea (Renfrew and Moore, 1999), the Great Lakes (Braham and Kristovich, 1996; Kristovich et al., 2000) as well as the Sea of Japan and the Sea of Okhotsk (Tusboki et al., 1989; Asuma et al., 1997; Inoue et al., 2003). Previous studies have highlighted the important role that vertical shear of the background wind

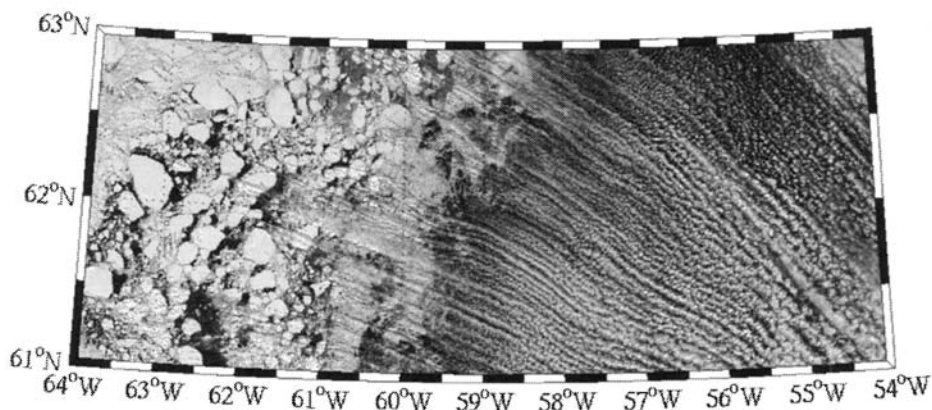


Figure 1. MODIS image on 12 April 2002 showing the organization of convection into two-dimensional roll clouds over and downstream of the marginal sea-ice zone of the Labrador Sea.

plays in the organization of the Rayleigh-Benard convection into two-dimensional roll clouds and the transition to three-dimensional cellular convection that occurs as the shear is eliminated through vertical momentum mixing (Asai, 1970; Sykes and Henn, 1989; Moeng and Sullivan, 1994; Khanna and Brasseur, 1998). The dramatic warming and moistening of the atmospheric boundary layer that occurs as a result of the air-sea interaction has also been documented (Hartmann et al., 1997; Renfrew and Moore, 1999; Brummer and Pohlmann, 2000). Much less is known about the impact that sea ice has on roll-cloud development, air-sea interaction and subsequent boundary-layer modification. Some studies have shown that air mass modification occurs over the sea ice (Brummer et al., 1994; Muller et al., 1999; Renfrew and Moore, 1999; Vihma and Brummer, 2002), but there is still much that is unknown regarding the specifics of air-sea interaction in the presence of heterogeneous sea-ice cover.

Numerical modelling, with its ability to document the spatial structure and temporal evolution of roll vortices, is an excellent tool with which to further our understanding of roll clouds and their impact on the atmospheric boundary layer. Making use of their two-dimensional nature, as revealed by satellite imagery, most early simulations used two-dimensional models with resolutions that were limited by available computing power (Mason and Sykes, 1982; Sykes and Henn, 1988; Raasch, 1990). These simulations successfully captured the two-dimensional aspects of the roll clouds; however, development in the downwind direction, such as the transition from rolls to cellular convection, could not be addressed. Recently high-resolution three-dimensional models have begun to be employed to simulate the development of roll clouds associated with high-latitude cold air outbreaks. The simulations Liu et al. (2004), which were performed in large domains at high spatial resolution, in particular have been successful in capturing the transition from two-dimensional roll convection to three-dimensional cellular convection.

Numerical simulations have also been performed on the atmospheric boundary-layer modification over the sea-ice zone. Based on observations from the Marginal Ice Zone Experiment (MIZEX) and the Coordinate Eastern Arctic Experiment (CEAREX), Guest et al. (1995) numerically investigated the wind stress variations within the marginal sea-ice zone and provided an improved method for implementing wind stress forcing over sea ice. Dare and Atkinson (1999; 2000) used a two-dimensional model to study the response of the atmospheric boundary layer to large leads and polynyas in the sea-ice zone of the Southern Ocean. They found a substantial moistening and warming of the boundary layer over and downstream of these inhomogeneities in the sea-ice cover. Pagowski and Moore (2001) implemented a parameterization of fractional sea-ice cover in a regional forecast model. They found that such a parameterization resulted in a

better agreement with the observations of Renfrew and Moore (1999) with respect to air-mass modification over the sea-ice zone and downstream over the open ocean during high-latitude cold air outbreaks. Vihma et al. (2003) simulated observed on-ice air flows over the Arctic Ocean marginal sea-ice zone, and the parameterization of drag coefficients that they developed agreed well with the observations. They also found that high vertical and horizontal resolution was necessary in simulations to reproduce the observations.

However, missing from all of these studies is a representation of the microphysical and small-scale dynamical processes that are responsible for the development of the roll and cellular clouds associated with high-latitude air-sea interaction in a domain large enough to include both an inhomogeneous sea-ice cover and the downstream ocean (e.g. Figure 1). This study attempts to rectify this situation through the use of a three-dimensional cloud resolving numerical model run at high resolution (0.5 km) over a large domain (100 km \times 400 km). One advantage of running such a model is the ability to explicitly represent inhomogeneities in the sea-ice cover, rather than parameterize them as has been done in the past (Pagowski and Moore, 2001; Schlunzen and Katzfey, 2003). It must be emphasized that with the horizontal resolution of the current simulation, we are unable to completely resolve all the scales of motion associated with these roll clouds, as can be more completely done with large-eddy simulations (LES) of boundary roll clouds (Muller et al., 1999). The advantage of the approach that we use is the ability to perform simulations in large domains that allow for the air-sea-ice interaction to occur over distances typically found in marginal ice zones, while still allowing the roll clouds to evolve over the open ocean. At present, this capability is not possible with LES models.

The aim of the present work is twofold: (1) to examine the development of boundary-layer roll clouds over the marginal sea-ice zone and the adjacent open water, and (2) to investigate the impact of variations in sea-ice concentration on atmospheric boundary-layer roll development. The remainder of this paper is organized as follows: the numerical model and experimental design are discussed in Section 2. The development of boundary-layer roll clouds over a marginal sea-ice zone with a linearly decreasing ice concentration is examined in Section 3. The impact of variations in sea-ice concentration on atmospheric boundary-layer roll development is discussed in Section 4. Finally, our results are summarized in section 5.

2. Numerical Model and Experimental Design

The model used in this study is the Cloud Resolving Storm Simulator (CReSS) developed at Nagoya University (Tsuboki and Sakakibara, 2002).

CReSS uses the non-hydrostatic and compressible equations of motion, a 1.5-order turbulent kinetic energy (TKE) closure scheme and a bulk method for cold rain, including water vapour, rain, cloud water, cloud ice, snow and graupel. Prognostic variables are three-dimensional velocity components, perturbation pressure and potential temperature as well as the mixing ratio for water vapour, and five species of hydrometeors. The model has been successfully used to simulate convective roll clouds during a cold-air outbreak over open water. (Liu et al., 2004) as well as a number of other convective weather systems (Tsuboki and Sakakibara, 2002).

The model domain used in these simulations was 400 km in the along roll (x) direction, 100 km in the cross roll (y) direction and 12 km in the vertical (z) direction; the horizontal grid interval was 500 m. In the vertical, grid stretching was applied with the interval varying from 25 m near the surface to approximately 1 km near the top of the domain. This resulted in a computational grid that was $800 \times 200 \times 60$ grid points. In the x direction, the first 50 km of the domain was specified to be land with a fixed temperature of -23°C ; the next 100 km was specified to be the sea-ice zone; while the remaining 250 km was specified to be open water with a fixed temperature of 3°C (Figure 2). Previous observations have shown that during cold air outbreaks intense surface heat and moisture fluxes force the atmospheric boundary layer to grow quickly, while the sea surface temperature is only slightly affected (Vihma et al., 2003); as a result, we use a fixed surface temperature. For all experiments, the model was initialized with a typical atmospheric sounding from a cold-air outbreak over the Labrador Sea, which shows dry and cold air with a significant low-level wind shear (Renfrew and Moore, 1999; Liu et al., 2004). The surface and initial conditions were homogeneous throughout the domain with the exception of the sea-ice zone where sea ice is randomly distributed in the y direction. Periodic boundary conditions were applied in the y direction, while wave radiation boundary conditions were applied in the x direction.

The high spatial resolution of the model allows us to use an explicit representation of sea ice. We assume that the ice is sufficiently thick so that there is no flux of heat from the underlying ocean surface and as a result, the ice covered grid points were assigned the same surface temperature as the land, while ice free grid points were assigned the same surface temperature as the open water. In addition, the ice covered grid points were assigned an aerodynamic roughness length (0.001 m) that was different from that of the grid points that were land (0.1 m). The roughness length over open water is a function of wind speed and is calculated based on results of Kondo (1975); for the parameter range under consideration here, the surface roughness over the ocean was on the order of 0.0001 m.

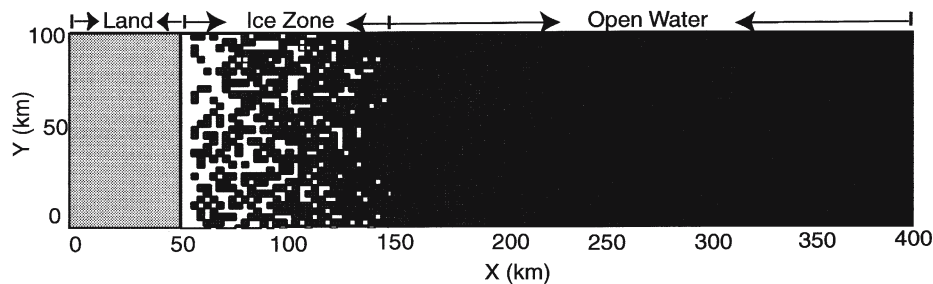


Figure 2. Schematic of the model domain used in this paper. The grid points covered with yellow indicate land; the grid points covered with white indicate sea ice; the grid points covered with blue indicate open water.

Observations of the marginal sea-ice zone typically show a complex heterogeneity in sea-ice concentration embedded in a trend towards lower ice concentration as one moves from the land towards the open ocean (Renfrew et al., 1999; Pagowski and Moore, 2001; Clement et al., 2004; Semmler et al., 2004). Motivated by satellite imagery (Figure 1), the variability in sea-ice concentration was assumed to occur on a 3-km length scale for this idealized study without detailed small-scale sea-ice variation (Haggerty et al., 2004). This is obviously a simplification of the complexity of scales that are observed, but we believe it is appropriate for a numerical simulation at this resolution and over this domain size. Four experiments with different sea-ice concentration schemes have been performed to investigate the effect that these inhomogeneities have on the atmospheric boundary layer and roll cloud development. In each instance, the sea-ice concentration was allowed to vary in a random fashion in the y direction but was prescribed in the x direction. Figure 2 shows an example of one of the sea-ice distributions employed in this paper. In this experiment, named Exp1, the sea-ice concentration decreased in a piecewise linear fashion in x from 100% ice cover at $x = 50$ km to 0% ice cover at $x = 150$ km. At each x , the fraction of ice covered grid points in y was randomly assigned, according to the prescribed piecewise linear trend. In addition to this, experiments were also run in which the sea-ice concentration was fixed for $50 < x < 150$ km at 40% (Exp2), 70% (Exp3) and 90% (Exp4), while randomly assigned in the y direction. In this set-up, the total sea-ice cover in experiments 1 and 2 are the same. It should be emphasized that no movement of the sea ice due to the imposed momentum stress was allowed in these experiments. Over the relatively short integration times of the experiments (typically 10 h) this assumption is a reasonable approximation.

3. Boundary-layer Roll Cloud Development Over and Downstream of the Sea-ice Zone

In this section the development of boundary-layer roll clouds, with a linearly decreasing sea-ice concentration are examined in detail (Exp1 – Figure 2). Solutions will be shown at a time of 10 h into the simulation. At this time, the flow had reached a quasi-steady equilibrium. In Figure 3, we present the model simulated three-dimensional structure of the specific humidity field. The figure shows a deepening boundary layer with a well-defined roll structure as one proceeds downstream along the axis (x) of the mean wind. The surface specific humidity increases from the coast to the ice edge, and then downstream over the open water, indicating that air-sea interaction is occurring within the sea-ice zone as well as over the open water. Within the first 50 km of the sea-ice zone, there exist anomalies in the humidity field that are the result of variations in sea-ice concentration (Figure 2) but no evidence of mesoscale organization. Approximately 50 km from the coast ($x = 100$ km), the humidity field starts to become organized into a two-dimensional structure, while further downstream ($x > 300$ km) there is a transition into a three-dimensional organization. This spatial evolution indicates that the vertical transport of heat and moisture takes place through different mechanisms in these three regions: subgrid-scale (i.e. homogeneous) turbulence for $50 \text{ km} < x < 100 \text{ km}$; roll convection for $100 \text{ km} < x < 300 \text{ km}$, and cellular convection for $x > 300 \text{ km}$. This is in good agreement with observations (Etling and Brown, 1993; Hartmann et al., 1997; Brummer, 1999; Renfrew and Moore, 1999).

The potential temperature field in the mean wind direction also shows that the boundary layer is warming and deepening with downstream distance from the sea ice to the open water (Figure 4). Note that there is a reduction in the near surface stratification over the sea-ice zone as well as over the open water that is consistent with observations (Brummer, 1996; Renfrew and Moore, 1999; Olsson and Harrington, 2000). There are significant ‘wiggles’ in the contours after $x = 300$ km, coincident with the transition from two-dimensional roll convection to three-dimensional cellular convection.

In Figure 5, we present a more detailed view of the evolution of the vertical profiles of potential temperature, specific humidity and zonal (i.e. x component) wind from the sea-ice zone to the open water. All three profiles show that the modification of the atmospheric boundary layer is occurring over the sea-ice zone as well as over the open water. There is a surface warming ($\approx 6^\circ\text{C}$), moistening ($\approx 0.6 \text{ g kg}^{-1}$) and an increase in wind speed ($\approx 6 \text{ m s}^{-1}$) in the boundary layer with downstream distance. These changes are vertically mixed throughout the boundary layer resulting in an increase in its depth with downstream distance. The mixing eliminates the

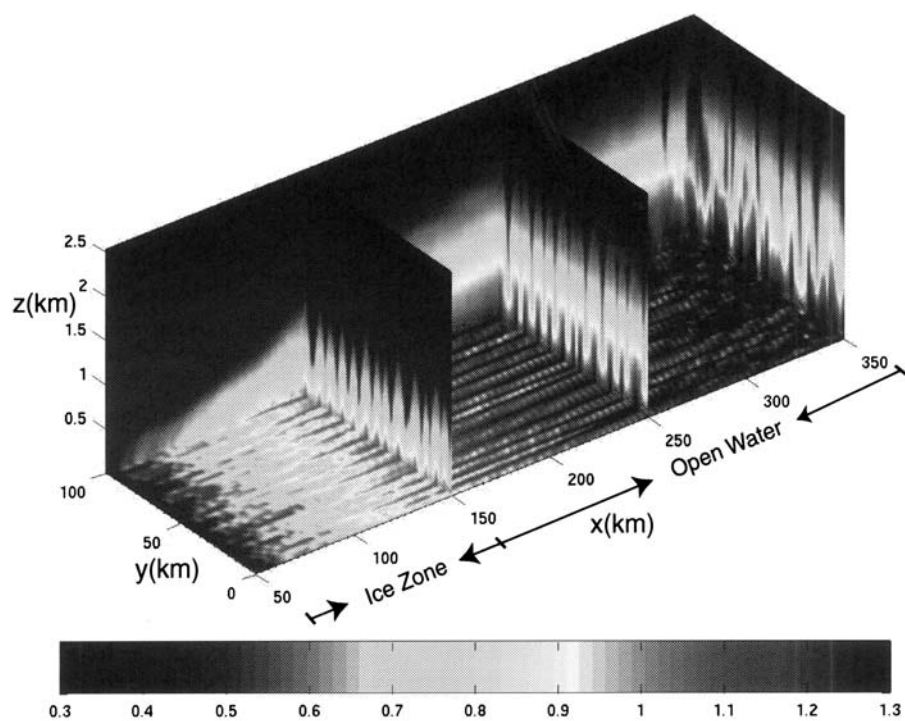


Figure 3. Three-dimensional display of the specific humidity (g kg^{-1}) field from the simulation at 10 h. The $x-z$ plane is at $y=100$ km; the $x-y$ plane is at $z=25$ m; three $y-z$ planes are at $x=150$ km, $x=250$ km and $x=350$ km separately.

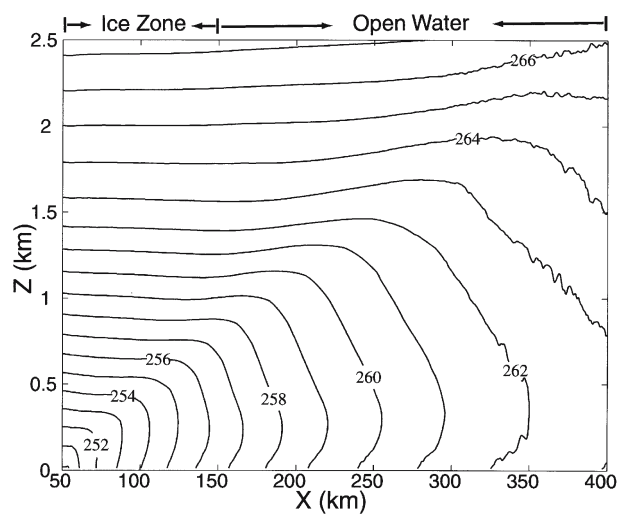


Figure 4. Vertical cross-section of potential temperature (K), averaged in the y direction, along the mean wind direction at 10 h.

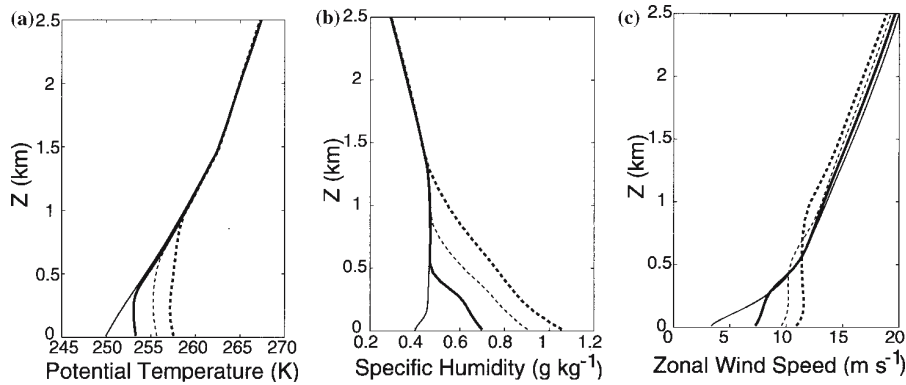


Figure 5. The evolution of vertical profiles of (a) potential temperature (K), (b) specific humidity (g kg^{-1}) and (c) zonal wind (m s^{-1}) at the $x=0$ km (thin solid), 90 km (thick solid), 130 km (thin dashed) and 170 km (thick dashed) separately after 10 h of model simulation. All profiles are averaged in the y direction.

vertical wind shear, a result that we suggest is responsible for the transition from two-dimensional roll convection to three-dimensional cellular convection (Figure 3). Figure 5a also shows that downstream of the ice zone, $x=170$ km, the lower layers of the atmosphere are still much colder than the ocean. Therefore the lower atmosphere is still very cold and dry, and a very strong temperature gradient exists in the surface layer, which is gradually removed by convection further downstream.

The structure and evolution of the roll clouds with downstream distance (or fetch), and their associated secondary flow, is illustrated in Figure 6. There is no evidence of an organized secondary flow at $x=90$ km (45% ice cover), but there exist small anomalies in the low-level humidity field (reaching a height of ≈ 500 m) and even some clouds that are the result of inhomogeneities in the sea ice (Figure 2). At $x=130$ km (18% ice cover), the roll vortices are well defined in cloud liquid water, specific humidity (q) and through a rotational secondary flow. At $x=170$ km (open water) the clouds are deeper, q is higher and the secondary flow is more substantial. In agreement with conceptual models and observations of high latitude roll clouds (Brummer et al., 1992; Renfrew and Moore, 1999), the secondary flow has intense and narrow updrafts with the highest humidity air near the centre of the updrafts. The periodic nature of the updrafts and the clouds that form over them provide the two-dimensional organization to the cloud field (e.g. Figure 1). In simulations performed without sea ice present (Hartmann et al., 1997; Weckwerth et al., 1997; Muller et al., 1999; Cooper et al., 2000; Liu et al., 2004), the wavelength in the cross-roll direction tends to be uniform. Here the wavelength is non-uniform varying

from 5 to 12 km, as a result of interactions between the developing roll clouds and inhomogeneities in the underlying sea-ice distribution.

In Figure 7a, we show the 10-m vector wind and the scalar wind speed fields. For visualization purposes, we have chosen to show only half of the domain in the cross roll direction. Convergence in the updrafts and divergence in the downdrafts, associated with the secondary flow (Figure 6), results in a clear modulation of the horizontal wind speed so as to be lower in areas of convergence and higher in areas of divergence. A similar roll structure in surface wind field has been captured in Synthetic Aperture Radar data (Bullock et al., 1997; Muller et al., 1999; Levy, 2001). There also exist inhomogeneities in wind speed over the sea-ice zone that are probably the result of the difference in surface roughness between sea ice and open water and the heterogeneous surface heating. Note that the rolls are almost parallel to the mean wind direction. The set-up of the model with periodic boundary conditions and no mean flow in the y direction eliminates the possibility of Ekman flow in the boundary layer and the observed turning of the rolls with respect to the mean wind (Etling and Brown, 1993).

In Figure 7b, we present the surface total turbulent heat flux, i.e. the sum of the latent and sensible heat fluxes, and the vector winds. Ice covered regions, where the flux is zero, are shown as white. The figure shows an increase in the magnitude of the heat flux as one moves from the land over the sea-ice zone and the ocean. Regions of low sea-ice concentration have higher heat fluxes, while the largest fluxes, in excess of 650 W m^{-2} , occur over the open water just downwind of the sea-ice zone. Beyond this region, there is a modest reduction in the magnitude of the fluxes, consistent with observations (Renfrew and Moore, 1999), which is a result of the warming and moistening of the boundary layer and the concomitant reduction in the air-sea temperature and humidity contrasts (Figure 5a and b). This reduction in the surface heat fluxes occurs despite the increase in low-level wind speed (Figure 5c). There is also a significant roll signature in the surface heat flux field, with smaller fluxes in the updrafts and larger fluxes in the downdrafts. This is a result of the secondary circulation (Figure 6), which results in a reduction in the humidity and temperature within the downdrafts and an increase in humidity and temperature within the updrafts. Higher wind speeds in the downdrafts (Figure 7a) also contribute to the elevated heat fluxes in the downdraft regions. The typical variation in heat fluxes is, for example at $x = 200 \text{ km}$: 570 W m^{-2} in an updraft and 640 W m^{-2} in a downdraft; or at $x = 300 \text{ km}$: 540 W m^{-2} in an updraft and 600 W m^{-2} in a downdraft. In other words, in this experiment, there is typically a modulation of $60\text{--}70 \text{ W m}^{-2}$ (10%) in the surface turbulent heat fluxes by the boundary-layer roll vortices.

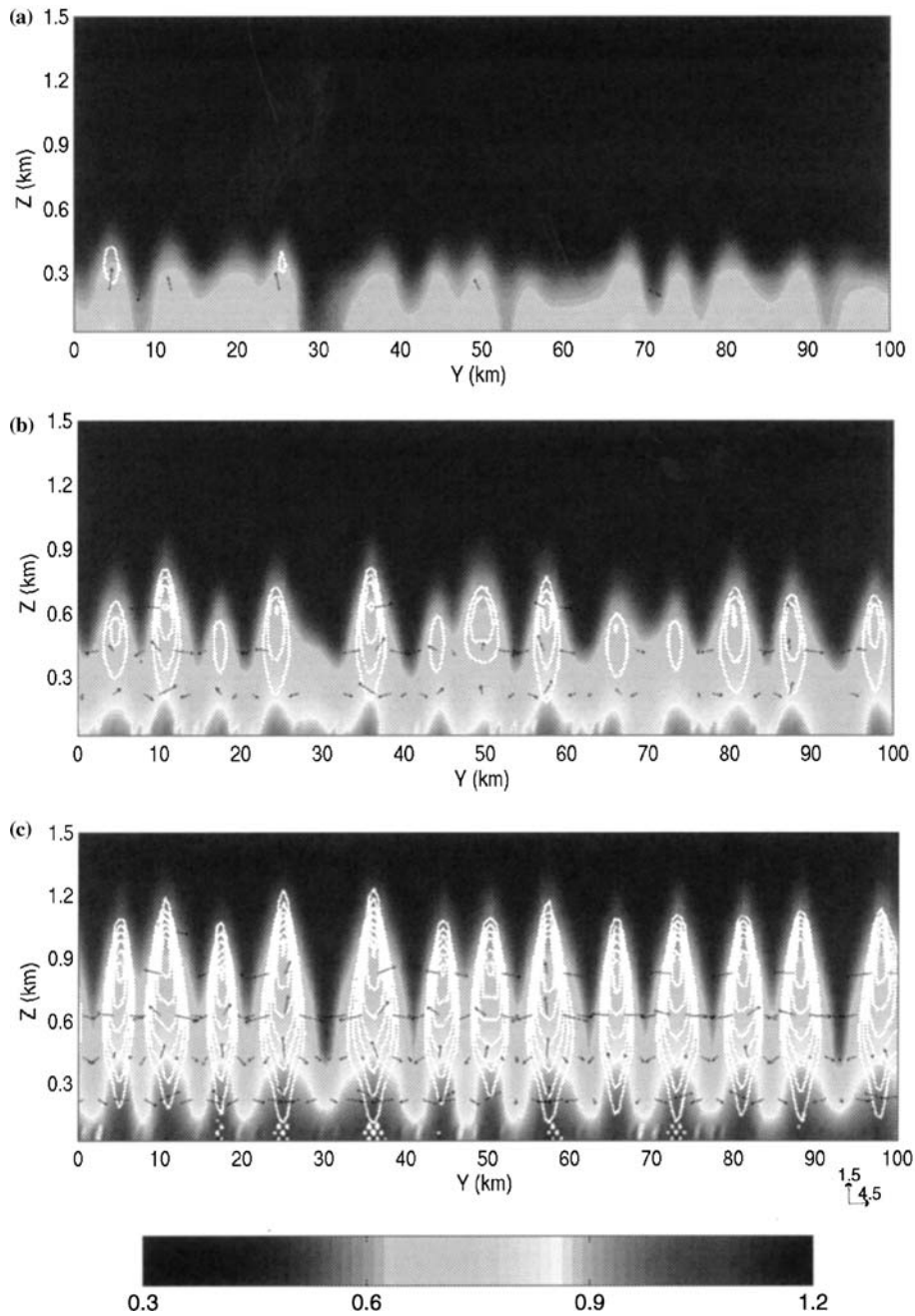


Figure 6. Secondary flow development at 10 h over the sea-ice zone at (a) $x = 90$ km (45% sea ice), (b) $x = 130$ km (18% sea ice) and (c) $x = 170$ km (open water). The specific humidity field (g kg^{-1}) is shaded, the cloud liquid water mixing ratio (g kg^{-1}) is contoured with contour interval 0.05 g kg^{-1} and the velocity in the $y-z$ plane is indicated by the vectors (only plotted every fourth grid in y direction and every third grid in z direction with $\text{abs}(w) > 0.1 \text{ m s}^{-1}$).

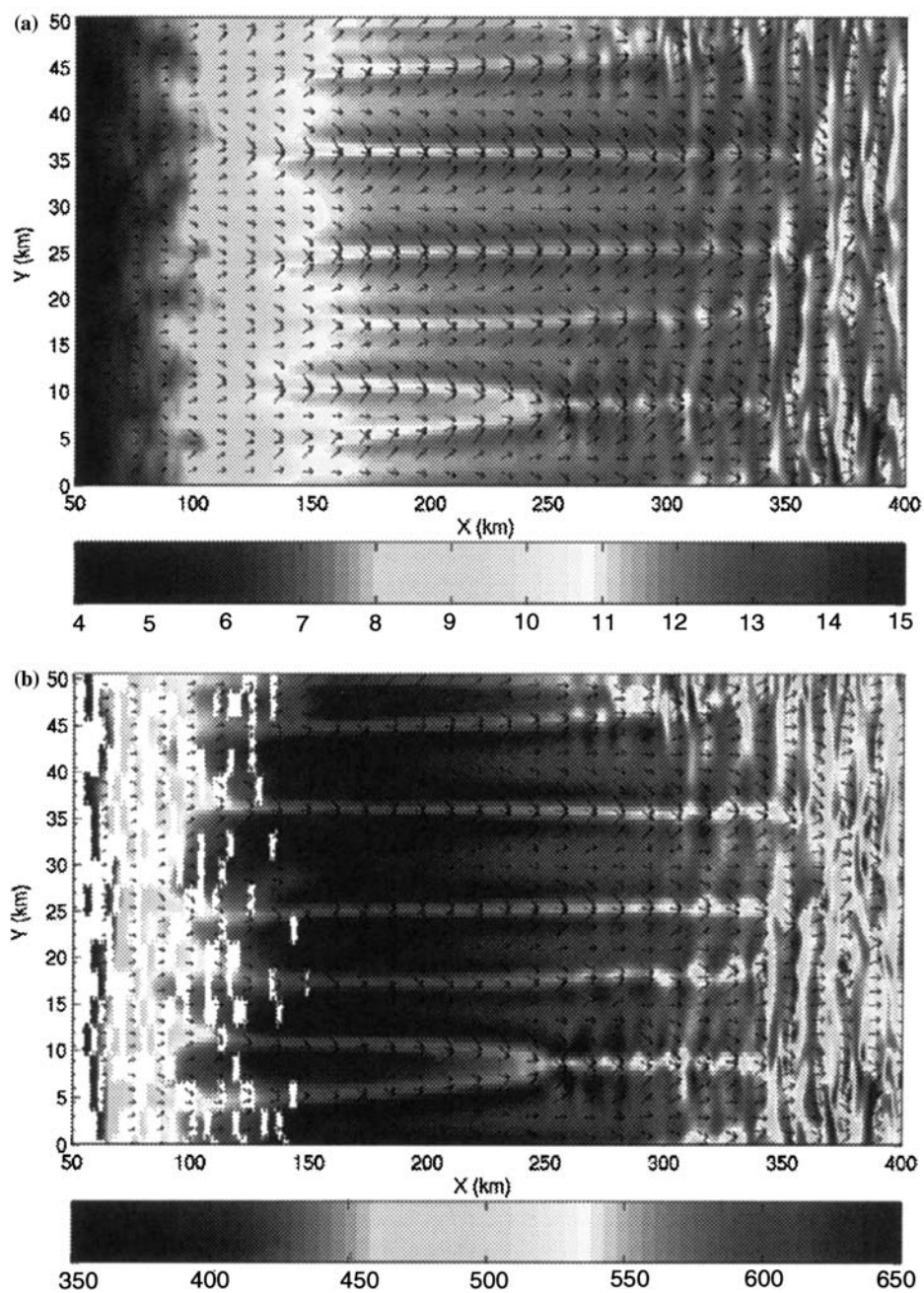


Figure 7. Horizontal cross-section of (a) horizontal wind at 10 m (m s^{-1}) and (b) surface total turbulent heat flux (W m^{-2}) at 10 h. The velocity in the $x - y$ plane is indicated by the vectors and only plotted every 24th grid in the x direction and every third grid in the y direction.

Figure 7 also shows a merging of the rolls with downstream distance, followed by a transition to cellular convection. This is consistent with observations and we believe that it is the result of the elimination of the vertical wind shear by the secondary flow (Figure 5c). These figures also indicate that the roll structure once developed is able to retain its organization even in the presence of sea ice. This is also a characteristic that has been observed (Figure 1).

In Figure 8, we present the cross-roll structure in vertical velocity and specific humidity fields at $x = 130$ km, $z = 0.5$ km; also indicated on the figure are those grid points that are ice covered. As seen in Figure 6 there is a positive correlation between updrafts and peaks in specific humidity. The modulations in specific humidity are qualitatively and quantitatively similar to observations of such cold-air outbreaks, for example, Figure 7 from Renfrew and Moore (1999). These results confirm that some updrafts with upward motion and large specific humidity do occur over the ice, and there is a large variation in the intensity of the updrafts. It is interesting to note that the basic wavelength of the rolls, in terms of vertical velocity, remains approximately constant over the cross-section, whereas the magnitude associated with individual rolls has quite a range, the peak to trough difference varying from $\approx 0.1 \text{ m s}^{-1}$ to $\approx 1.5 \text{ m s}^{-1}$. A similar variation can be seen in the specific humidity. We would suggest that it is an interaction between the roll vortices and the underlying heterogeneous sea-ice cover that is the primary cause of the modification of the roll vortex signature. For example, areas of low ice concentration will enable higher latent heat fluxes, leading to stronger secondary flow, and so more latent heat release through condensation in the roll updrafts. This idea is corroborated by a previous series of experiments without sea ice, where the boundary-layer roll clouds that developed were more uniform in magnitude (Liu et al., 2004), and is discussed further in the next section.

4. A Comparison of Experiments with Various Sea-ice Distributions

In this section, the results from experiments with various sea-ice concentrations but the same upstream atmospheric profile will be examined to investigate the effect of sea-ice concentration on the evolution of atmospheric boundary-layer variables and roll structures. Please refer to Section 2 for a detailed description of the design of the experiments. The evolution of potential temperature, specific humidity, cloud mixing ratio (the sum of cloud water and cloud ice) and precipitation rate with downstream distance for various sea-ice concentrations is provided in Figure 9. The figure shows that the sea-ice concentration has a significant impact on the spatial variation of the above variables, both over the sea-ice zone and further

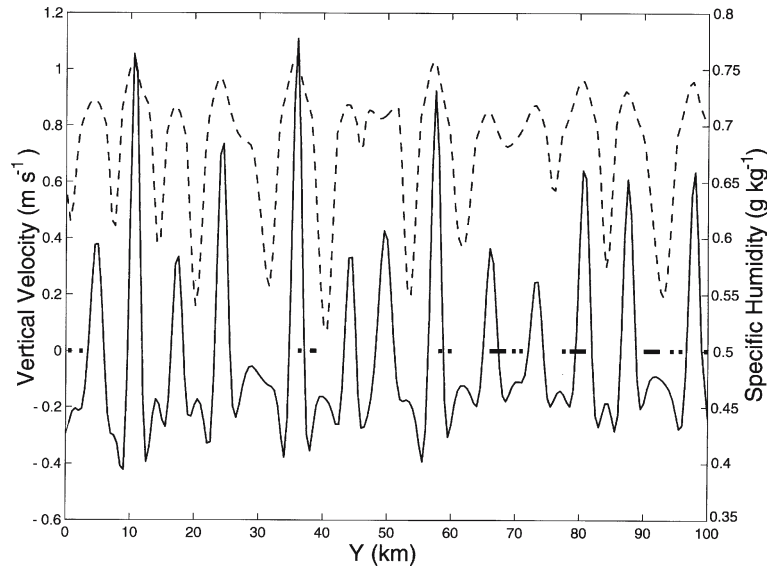


Figure 8. Cross-roll structure in vertical velocity (m s^{-1} , solid line) and specific humidity (g kg^{-1} , dashed line) fields at $x = 130 \text{ km}$, $z = 0.5 \text{ km}$. The thick solid line indicates surface ice cover.

downstream. In all cases, there exists a clear signature of the transition from the sea-ice zone to open water at $x = 150 \text{ km}$. This is the result of the removal of the insulating effect of the sea ice and the resulting increase in air-sea heat exchange. The abruptness of the signature is reduced for the experiments that allow for some of the interaction to occur over the sea-ice zone. As one might expect, lower sea-ice concentrations result in warmer and more humid air with increased cloud formation and more intense precipitation over the sea-ice zone and, to an extent, downstream. In Exp4, with a 90% sea-ice concentration, no clouds or precipitation occur over the sea-ice zone ($50 < x < 150 \text{ km}$), and it would seem that with such a high ice concentration, the moisture flux is too low to allow cloud formation over the sea-ice zone. There appears to be a gradual transition from cloud to no cloud over the sea-ice zone as the sea-ice concentration is increased from 40 to 70% (Exps 2 and 3). In Exps 2 and 3 there is a rapid warming and moistening of the atmosphere as well as cloud formation and precipitation at or just downstream of the ice edge. Such a sharp change at the ice edge is the result of a thermal internal boundary-layer development caused by the discontinuity in the surface conditions, as has been observed and simulated using simple slab mixed-layer models (Venkatram, 1977; Renfrew and King, 2000). Generally the differences between the simulations gradually diminish further downstream, which indicates that the atmosphere has

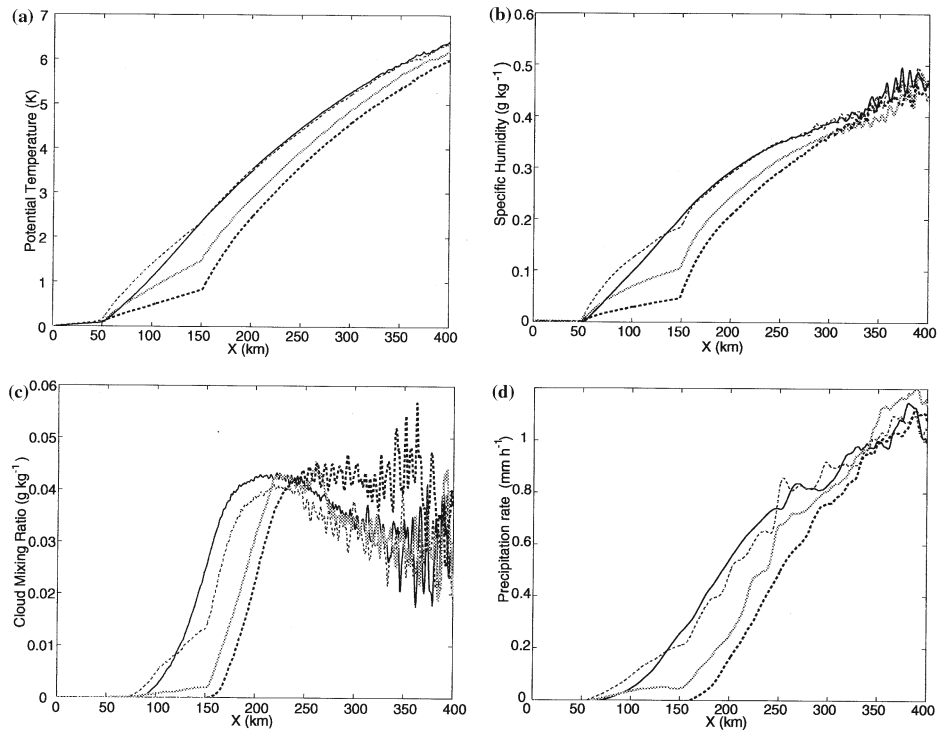


Figure 9. Variation of (a) potential temperature (K), (b) specific humidity (g kg^{-1}), (c) cloud mixing ratio (g kg^{-1}) and (d) precipitation rate (mm h^{-1}) as a function of distance downwind (x) at 10 h for Exp1 (black), Exp2 (red), Exp3 (green) and Exp4 (Blue). All the variables represent anomalies from the upstream conditions and are averaged from the surface to 2 km in the vertical then averaged along the y direction.

only a partial and limited memory of the impact of different sea-ice concentrations.

Figure 10 shows the roll structure represented in the horizontal cross-section of the cloud liquid water field at $z = 1$ km. It can be seen that the roll clouds start to appear at different locations along the mean wind direction, and the wavelength of the roll clouds is different among the simulations. The cloud streets appear at ≈ 50 km further downstream in the simulation with high sea-ice concentration (Exp4) as compared to the control experiment (Exp1). The cloud streets with the largest wavelength are formed in Exp3 (70% sea-ice concentration). The cloud streets with the smallest wavelength are formed in Exp4 (90% sea-ice concentration). The most uniform roll clouds are those of Exp1 and Exp4, where the sea-ice distribution decrease linearly with fetch and where there is 90% ice cover. In Exps 2 and 3 where there is a more even mix between sea-ice grid points and open water grid points, the roll clouds appear less regular, the

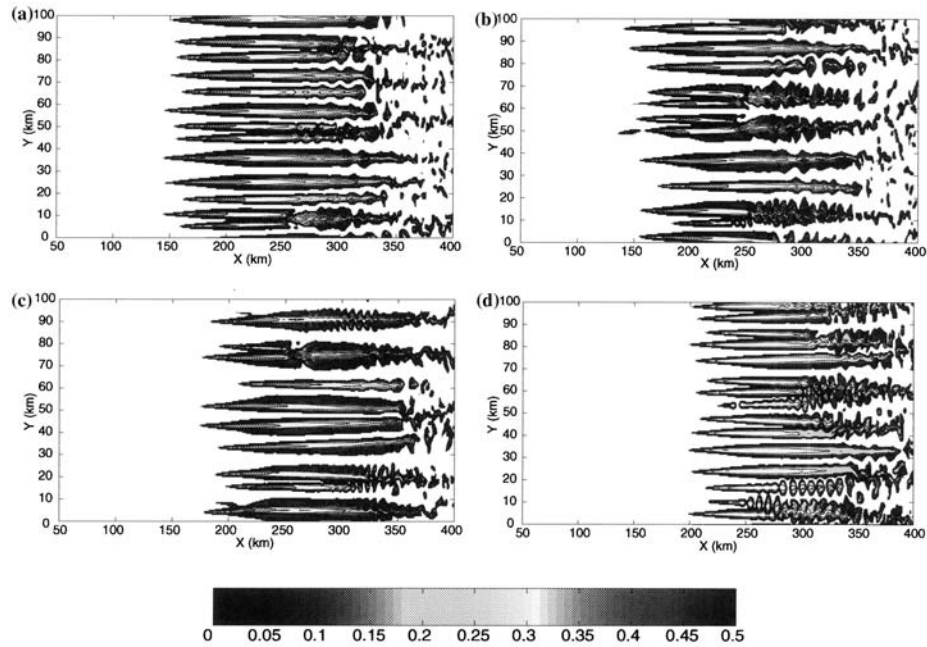


Figure 10. Horizontal cross-section of cloud mixing ratio (g kg^{-1}) at $z = 1000$ m at 10 h for (a) Exp1, (b) Exp2, (c) Exp3, (d) Exp4.

wavelength is larger and there appears to have been more roll mergers. It appears these more random distributions of sea ice lead to a more ‘chaotic’ roll cloud development.

It is also noted that for Exp1 and Exp2 (the experiments with same total sea-ice concentration but different spatial distributions) the evolution of potential temperature and specific humidity is similar but there are still differences in the evolution of the cloud mixing ratio and precipitation rate (Figure 9). The cloud mixing ratio and precipitation rate are generally higher in the more realistic Exp1 than in Exp2. The difference between these two experiments reflects the fact that the thermodynamical and dynamical processes associated with cloud formation and precipitation are highly non-linear and so the spatial distribution of sea ice, which results in variations in the vertical transport pattern of heat and moisture, leads to different downstream development.

The secondary flow intensity associated with the roll structures is also different amongst the simulations (Figure 11a). The evolution of the secondary flow momentum indicates the roll vortices are more intense and form earlier in the simulations with lower sea-ice concentration. Further downstream, starting around $x = 300$ km, cellular convection starts to dominate the convection and there are large fluctuations in the secondary flow

momentum. The evaluation of the boundary-layer Rayleigh number, Ra (defined below in Equation (1)), along the mean wind direction shows that the Rayleigh–Benard convection gradually develops over the sea-ice zone and reaches a maximum at the ice edge in all the simulations (Figure 11b). Again the simulations with lower sea-ice concentration result in a high Rayleigh number, i.e. more intense convection. It should also be noted that the sudden change of surface forcing as the air moves from 90% ice cover in the sea-ice zone to totally open water, results in the sharpest increase of convection intensity near the ice edge in Exp4. Here, the Rayleigh number is defined

$$Ra = \frac{g\alpha\Delta T d^3}{\nu\kappa}, \quad (1)$$

in which g is the acceleration of gravity (9.8 m s^{-2}), α is the thermal expansion coefficient ($3.0 \times 10^{-3} \text{ K}^{-1}$), ΔT vertical temperature difference in the distance of d , ν is the kinematic viscosity ($1.4 \times 10^{-5} \text{ m}^2 \text{ s}^{-1}$), and κ is the thermal diffusivity ($2.0 \times 10^{-5} \text{ m}^2 \text{ s}^{-1}$). The Rayleigh number is calculated between each vertical level and then averaged within the boundary layer, the top of which is defined by the inversion height, and which in this case varies from about 200 m near the ice edge to over 1 km downstream over the open water.

An important field that characterizes the intensity of boundary-layer convection is the turbulent kinetic energy (TKE), which is directly related to the transport of heat, moisture and momentum throughout the boundary layer. In Figure 12, we show vertical cross-sections of TKE with downstream distance, averaged in the y direction. This figure shows that there exist clear differences in the evolution of TKE that result from variability in the sea-ice concentration. In general, the TKE is higher over the sea-ice zones with smaller sea-ice concentration. In Exp1 there is an approximately linear increase in TKE throughout the sea-ice zone, whereas in Exp2 the TKE increases rapidly to $\approx 0.7 \text{ m}^2 \text{ s}^{-2}$ near the start of sea-ice zone and then remains at this level throughout the rest of the zone. This clearly shows that TKE generation is related to the exact details of the sea-ice distribution. In Exp4, with 90% sea-ice concentration, there is only a very small amount of TKE produced over the sea-ice zone and this results in no significant secondary flow development there. In contrast, there is a sharp increase of TKE at the ice edge, which is a result of a sudden increase in the intensity of Rayleigh–Benard convection as the air reaches the open water.

In Figure 13, we present the evolution with downstream distance of sensible heat flux, latent heat flux and total turbulent heat flux for all four experiments. The heating and moistening of the atmospheric boundary layer over the sea-ice zone is significantly different among the simulations,

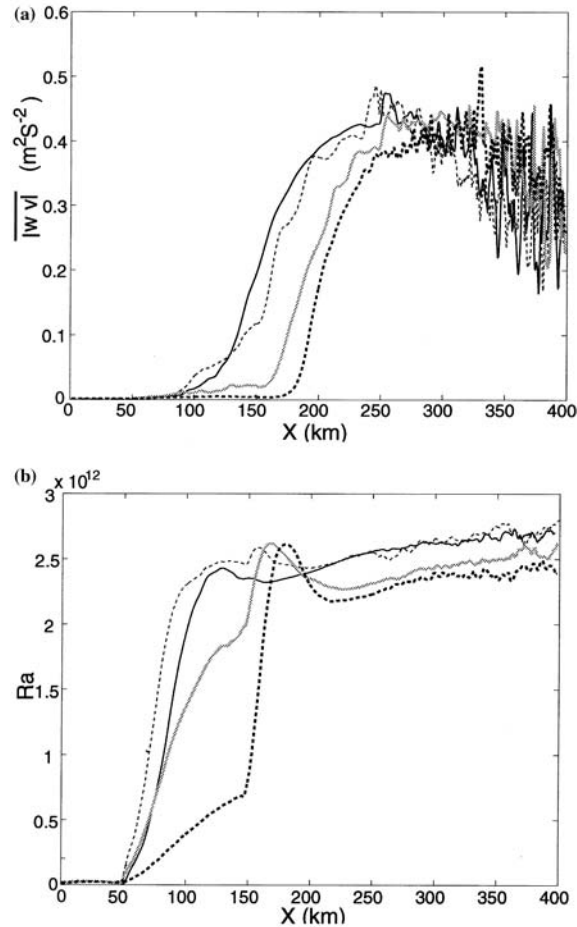


Figure 11. Averaged profiles as a function of along mean wind distance at 10 h for (a) secondary flow moment (averaged from the surface to 2 km in the vertical then averaged along the y direction) and (b) boundary-layer Rayleigh number (averaged along the y direction). Exp1 (black), Exp2 (red), Exp3 (green) and Exp4 (Blue).

while further downstream the differences are diminished. In Exp1 the increase in surface fluxes is approximately linear with fetch, mimicking the sea-ice concentration, and consistent with the observations of Renfrew and Moore (1999). In Exps 2, 3 and 4 there is a small increase in the fluxes with fetch through the sea-ice zone due to an increase in surface wind speed, before a large jump at the edge of the sea-ice zone. In all the simulations the latent heat flux is smaller than the sensible heat flux and the total heat fluxes reach a maximum over 600 W m^{-2} near the ice edge, which is in good agreement with observational results (Brummer, 1996; Renfrew and Moore, 1999). Interestingly, downstream over the open ocean, the latent

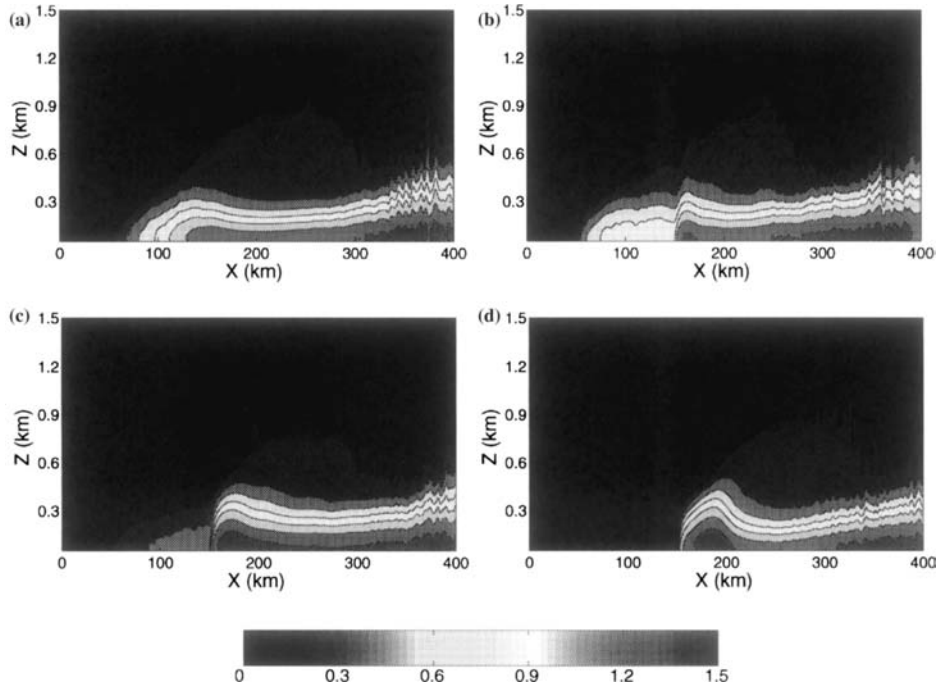


Figure 12. Vertical cross-sections of subgrid turbulent kinetic energy ($\text{m}^2 \text{s}^{-2}$) at 10h for (a) Exp1, (b) Exp2, (c) Exp3 and (d) Exp4. Averaged along the y direction.

heat fluxes converge to similar values for all four experiments, whereas the sensible heat fluxes for Exps 1 and 2, which peak rather closer to the ice edge, tend to be around 40 W m^{-2} lower than those of Exps 3 and 4. The approximately linear decrease in sensible heat flux is the result of the warming of the atmospheric boundary layer outweighing any modest increases in the surface wind speed (see Figures 9a and 7a), and is qualitatively consistent with observations (Renfrew and Moore, 1999). In contrast, the latent heat fluxes are approximately constant with fetch over this domain, again consistent with observations (Renfrew and Moore, 1999). This may be the result of the secondary flow that continues to replenish the atmospheric boundary layer with dryer air from above, as well as the warming of the boundary layer leading to a decrease in relative humidity, allowing continued moisture fluxes.

5. Conclusions

In this study, we have numerically investigated the effect that heterogeneity in sea-ice cover has on the development of boundary-layer roll clouds

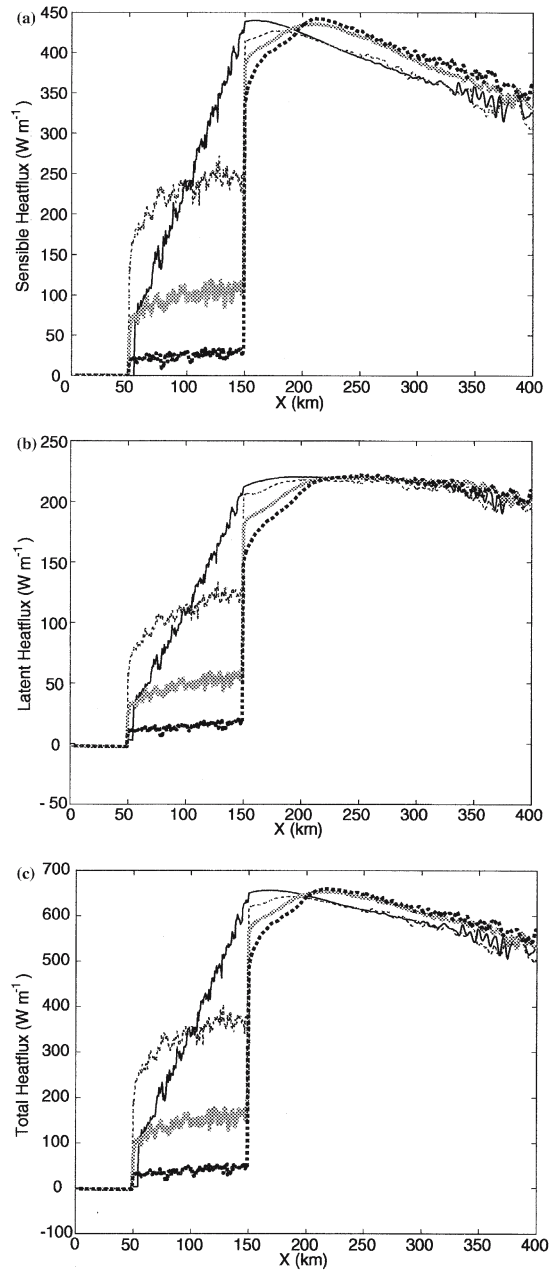


Figure 13. Evolution of (a) sensible heat flux (W m^{-2}), (b) latent heat flux (W m^{-2}), and (c) total heat flux (W m^{-2}) as a function of distance downwind (x) at 10 h for Exp1 (black), Exp2 (red), Exp3 (green) and Exp4 (Blue). All the variables are averaged along the y direction.

during cold air outbreaks. The study represents the first time that such simulations have been performed at sufficiently high spatial resolution to resolve the individual convective roll clouds, by allowing for a more realistic representation of dynamic and thermodynamic processes, and in a large enough domain to cover both the sea-ice zone and the downstream ocean, so as to allow for the continuous development of the boundary layer and roll clouds. The high spatial resolution of the simulations also allows for an explicit representation of heterogeneity within the sea-ice zone.

In agreement with observations, the results presented in this paper show that the vertical transport of heat and moisture can be divided into three regimes: subgrid-scale turbulence, roll convection and cellular convection. A detailed investigation of the evolution of the atmospheric variables at various locations over the sea-ice zone indicates that the atmospheric boundary layer starts to be warmed and moistened over the sea-ice zone, which suggests that sea ice and its variability plays an important role in modifying the atmospheric boundary layer during cold air outbreaks. For the lower sea-ice concentrations (Exp1, Exp2 and an extent Exp3) roll clouds begin to form over the sea-ice zone and become more mature and well-organized further downstream near the ice edge and over the open water. Sea-ice concentration has a significant impact on the characteristics of the roll clouds, in particular with respect to cross-roll wavelength and secondary flow intensity of the rolls. The sea-ice concentration also affects the vertical heat and moisture transfers in the simulations, and thus the surface turbulent heat fluxes.

The differences between the experiments generally diminish with downstream distance, which indicates that the atmosphere has only a partial and limited memory of the impact of different sea-ice concentrations. For the experiments with the same amount of total sea-ice concentration, but with different spatial distributions (Exp1 and Exp2), there are still differences in the development of cloud mixing ratio and precipitation rate, as well as in the roll development over the sea ice zone and adjacent downstream open water. This result suggests realistic representations of processes over the sea-ice zone are needed to properly calculate the associated energy and mass exchange budgets in current climate models, as these have shown a sensitivity to sea-ice concentration (Rind et al., 1997; Parkinson et al. 2001; Alexander et al., 2004). In this study, the atmospheric model is employed with fixed surface conditions, which is reasonable for a short-term simulation. A coupled model with a sea-ice model and ocean circulation embedded would be able to simulate the sea-ice melting, drift and surface temperature variation, and therefore provide a more realistic simulation of the complicated interaction between atmosphere, sea ice and ocean at high latitudes.

Acknowledgements

Funding for this research was provided by the Canadian Foundation for Climate and Atmospheric Sciences. The authors would like to thank Mr. A. Sakakibara of Chuden CTI Co., Ltd for his help in the use of CReSS. The helpful comments of reviewers also served to improve the manuscript.

References

- Alexander, M. A., Bhatt, U. S., Walsh, J. E., Timlin, M.S., Miller, J. S., and Scott, J. D.: 2004, 'The Atmospheric Response to Realistic Arctic Sea Ice Anomalies in an AGCM during Winter', *J. Climate* **17**, 890–905.
- Asai, T.: 1970, 'Three Dimensional Features of Thermal Convection in a Plane Couette Flow', *J. Meteorol. Soc. Japan* **48**, 18–29.
- Asuma, Y., Kikuchi, K., and Uyeda, H.: 1997, 'Organizations and the Interior Characteristics of Winter Monsoon Clouds by Dual-Polarization Doppler Radar Observation in Hokuriku, Japan', *Atmos. Res.* **43**, 297–314.
- Braham, R. R. and Kristovich, D. A. R.: 1996, 'On Calculating the Buoyancy of Cores in a Convective Boundary Layer', *J. Atmos. Sci.* **53**, 654–658.
- Brummer, B.: 1996, Boundary-layer modification in wintertime cold-air outbreaks from the arctic sea ice. *Boundary-Layer Meteorol.* **80**, 109–125.
- Brummer, B.: 1997, Boundary Layer Mass, Water, and Heat Budgets in Wintertime Cold-air Outbreaks from the Arctic Sea Ice. *Mon. Wea. Rev.* **125**, 1824–1837.
- Brummer, B.: 1999, Roll and Cell Convection in Wintertime Arctic Cold-air Outbreaks. *J. Atmos. Sci.* **56**, 2613–2636.
- Brummer, B. and Pohlmann, S.: 2000, Wintertime Roll and Cell Convection over Greenland and Barents Sea Regions: A Climatology. *J. Geophys. Res.* **105**, 15559–15566.
- Brummer, B., Thiemann, S.: 2002, The Atmospheric Boundary Layer in an Arctic Wintertime On-ice Air Flow. *Boundary-Layer Meteorol.* **104**, 53–72.
- Brummer, B., Rump, B., and Kruspe, G.: 1992, 'A Cold Air Outbreak near Spitsbergen in Springtime – Boundary-Layer Modification and Cloud Development', *Boundary-Layer Meteorol.* **61**, 13–46.
- Brummer, B., Busack, B., Hoerber, H., and Kruspe, G.: 1994, 'Boundary-Layer Observations over Water and Arctic Sea-Ice During on-Ice Air-Flow', *Boundary-Layer Meteorol.* **68**, 75–108.
- Bullock, R. J., Voles, R., Currie, A., Griffiths, H. D., and Brennan, P. V.: 1997, 'Two-look Method for Correction of Roll Errors in Aircraft-Borne Interferometric SAR', *Electronics Lett.* **33**, 1581–1583.
- Clement, J. L., Cooper, L. W., and Grebmeier, J. M.: 2004, 'Late Winter Water Column and Sea Ice Conditions in the Northern Bering Sea', *J. Geophys. Res.* **109**, C03022, doi:10.1029/2003JC002047.
- Cooper, K. A., Hjelmfelt, M. R., Derickson, R. G., Kristovich, D. A. R., and Laird, N. F.: 2000, 'Numerical Simulation of Transitions in Boundary Layer Convective Structures in a Lake-effect Snow Event', *Mon. Wea. Rev.* **128**, 3283–3295.
- Dare, R. A. and Atkinson, B. W.: 1999, 'Numerical Modelling of Atmospheric Response to Polynyas in the Southern Ocean Sea Ice Zone', *J. Geophys. Res.* **104**, 16691–16708.

- Dare, R. A. and Atkinson, B. W.: 2000, 'Atmospheric Response to Spatial Variations in Concentration and Size of Polynyas in the southern Ocean Sea-ice Zone', *Boundary-Layer Meteorol.* **94**, 65–88.
- Etling, D. and Brown R. A.: 1993, Roll Vortices in the Planetary Boundary-Layer - a Review. *Boundary-Layer Meteorol.* **65**, 215–248.
- Grotzner, A., Sausen, R., and Claussen, M.: 1996, 'The Impact of Sub-grid Scale Sea-ice inhomogeneities on the Performance of the Atmospheric General Circulation Model ECHAM3', *Clim. Dynamics* **12**, 477–496.
- Guest, P. S., Glendening, J. W., and Davidson, K. L.: 1995, 'An Observational and Numerical Study of Wind Stress Variations within Marginal Ice Zones', *J. Geophys. Res.* **100**, 10887–10904.
- Hartmann, J., Kottmeier, C., and Raasch, S.: 1997, 'Roll Vortices and Boundary-layer Development during a Cold Air Outbreak', *Boundary-Layer Meteorol.* **84**, 45–65.
- Haggerty, J. A., Maslanik, J. A., and Curry, J. A.: 2003, 'Heterogeneity of Sea Ice Surface Temperature at SHEBA from Aircraft Measurements', *J. Geophys. Res.* **108**, C10 8052, doi: 10.1029/2000JC000560.
- Inoue, J., Ono, J., Tachibana, Y., Honda, M., Iwamoto, K., Fujiyoshi, Y., and Takeuchi, K.: 2003, 'Characteristics of Heat Transfer over the Ice Covered Sea of Okhotsk during Cold-air Outbreaks', *J. Meteorol. Soc. Japan* **81**, 1057–1067.
- Khanna, S. and Brousseau, J. G.: 1998, 'Three-dimensional Buoyancy-and Shear-induced Local Structure of the Atmospheric Boundary Layer', *J. Atmos. Sci.* **55**, 710–743.
- Kondo, J.: 1975, 'Air-sea bulk transfer coefficients in diabatic conditions', *Boundary-Layer Meteorol.* **9**, 91–112.
- Kristovich, D. A., R., Young, G. S., Verlinde, J., Sousounis, P. J., Mourad, P., Lenschow, D., Rauber, R. M., Ramamurthy, M. K., Jewett, B. F., Beard, K., Cutrim, E., DeMott, P. J., Eloranta, E. W., Hjelmfelt, M. R., Kreidenweis, S. M., Martin, J., Moore, J., Ochs, H. T., Rogers, D. C., Scala, J., Tripoli, G., and Young, J.: 2000, 'The Lake-Induced Convection Experiment and the Snowband Dynamics Project', *Bull. Amer. Meteorol. Soc.* **81**, 519–542.
- Levy, G.: 2001, 'Boundary Layer Roll Statistics from SAR', *Geophys. Res. Lett.* **28**, 1993–1995.
- Liu, A. Q., Moore, G. W. K., Tsuboki, K., and Renfrew, I. A.: 2004, 'A High-resolution Simulation of Convective Roll Clouds during a Cold-air Outbreak', *Geophys. Res. Lett.* **31**, L03101, doi:10.1029/2003GL018530.
- Marshall, J., Dobson, F., Moore, K., Rhines, P., Visbeck, M., d'Asaro, E., Bumke, K., Chang, S., Davis, R., Fischer, K., Garwood, R., Guest, P., Harcourt, R., Herbaut, C., Holt, T., Lazier, J., Legg, S., McWilliams, J., Pickart, R., Prater, M., Renfrew, I., Schott, F., Send, U., Smethie, W., and Grp, L. S.: 1998, 'The Labrador Sea deep Convection Experiment', *Bull. Amer. Meteorol. Soc.* **79**, 2033–2058.
- Mason, P. J. and Sykes, R. I.: 1982, 'A Two-Dimensional Numerical Study of Horizontal Roll Vortices in an Inversion Capped Planetary Boundary-Layer', *Quart. J. Roy Meteorol. Soc.* **108**, 801–823.
- Moeng, C. H. and Sullivan, P. P.: 1994, 'A Comparison of Shear-Driven and Buoyancy-Driven Planetary Boundary-Layer Flows', *J. Atmos. Sci.* **51**, 999–1022.
- Moore, G. W. K., Reader, M. C., York, J., and Sathiyamoorthy, S.: 1996, 'Polar Lows in the Labrador Sea—A Case Study', *Tellus A* **48**, 17–40.
- Mourad, P. D. and Walter, B. A.: 1996a, 'Viewing a Cold Air Outbreak using Satellite-based Synthetic Aperture Radar and Advanced Very High Resolution Radiometer Imagery', *J. Geophys. Res.* **101**, 16391–16400.

- Mourad, P. D. and Walter, B. A.: 1996b, 'Analysis of Mesoscale Linear Features Observed in the Arctic Atmospheric Boundary Layer', *Mon. Wea. Rev.* **124**, 1924–1940.
- Muller, G., Brummer, B., and Alpers, W.: 1999, 'Roll-Convection Within an Arctic Cold-air Outbreak: Interpretation of In situ Aircraft Measurements and Spaceborne SAR Imagery by a Three-dimensional Atmospheric Model', *Mon. Wea. Rev.* **127**, 363–380.
- Olsson, P. Q. and Harrington, J. Y.: 2000, 'Dynamics and Energetics of the Cloudy Boundary Layer in Simulations of Off-ice Flow in the Marginal Ice Zone', *J. Geophys. Res.* **105**, 11889–11899.
- Pagowski, M. and Moore, G. W. K.: 2001, 'A Numerical Study of an Extreme Cold-air Outbreak over the Labrador Sea: Sea Ice, Air–sea Interaction, and Development of Polar Lows', *Mon. Wea. Rev.* **129**, 47–72.
- Parkinson, C. L., Rind, D., Healy, R. J., and Martinson, D. G.: 2001, 'The Impact of Sea Ice Concentration Accuracies on Climate Model Simulations with the GISS GCM', *J. Climate* **14**, 2606–2623.
- Raasch, S.: 1990, 'Numerical-Simulation of the Development of the Convective Boundary-Layer During a Cold Air Outbreak', *Boundary-Layer Meteorol.* **52**, 349–375.
- Rasmussen, E. A. and Turner, J.: 2003, *Polar Lows: Mesoscale Weather Systems in the Polar Regions*, 1st ed. Cambridge University Press, Cambridge, U.K., 645 pp.
- Renfrew, I. A. and Moore, G. W. K.: 1999, 'An Extreme cold-Air Outbreak over the Labrador Sea: Roll Vortices and Air–sea Interaction', *Mon. Wea. Rev.* **127**, 2379–2394.
- Renfrew, I. A. and King, J. C.: 2000, 'A Simple Model of the Convective Internal Boundary Layer and its Application to Surface Heat Flux Estimates within Polynyas', *Boundary-Layer Meteorol.* **94**, 335–356.
- Renfrew, I. A., Moore, G. W. K., Holt, T. R., Chang, S. W., and Guest, P.: 1999, 'Mesoscale Forecasting during a Field Program: Meteorological Support of the Labrador Sea Deep Convection Experiment', *Bull. Amer. Meteorol. Soc.* **80**, 605–620.
- Rind, D., Healy, R., Parkinson, C., and Martinson, D.: 1997, 'The role of sea ice in 2xCO(2) Climate Model Sensitivity. 2. Hemispheric Dependencies', *Geophys. Res. Lett.* **24**, 1491–1494.
- Schlunzen, K. H. and Katzfey, J.: 2003, 'Relevance of Sub-grid-Scale Land-use Effects for Mesoscale Models', *Tellus A* **55**, 232–246.
- Semmler, T., Jacob, D., Schlunzen, K. H., and Podzun, R.: 2004, 'Influence of Sea Ice Treatment in a Regional Climate Model on boundary Layer Values in the Fram Strait Region', *Mon. Wea. Rev.* **132**, 985–999.
- Sykes, R. I. and Henn, D. S.: 1988, 'On the Numerical Computation of Two-Dimensional Convective Flow', *J. Atmos. Sci.* **45**, 1961–1964.
- Sykes, R. I. and Henn, D. S.: 1989, 'Large-Eddy Simulation of Turbulent Sheared Convection', *J. Atmos. Sci.* **46**, 1106–1118.
- Tsuboki, K. and Sakakibara, A.: 2002, 'Large-scale Parallel Computing of Cloud Resolving Storm Simulator', in P. Z. Hans, K. Joe, M. Sato, Y. Seo, and M. Schimasaki (Eds.), *High performance computing*, 103 ed. Springer, 564 pp.
- Tsuboki, K., Fujiyoshi, Y., and Wakahama, G.: 1989, 'Structure of Land Breeze and Snow-fall Enhancement at the Leading Edge', *J. Meteorol. Soc. Japan*, **67**, 757–770.
- Venkatram, A.: 1977, 'A Model of Internal Boundary-Layer Development', *Boundary-Layer Meteorol.* **11**, 419–437.
- Vihma, T. and Brummer, B.: 2002, 'Observations and Modeling of the On-ice and Off-ice Air flow over the Northern Baltic Sea', *Boundary-Layer Meteorol.* **103**, 1–27.
- Vihma, T., Hartmann, J., and Lupkes, C.: 2003, 'A Case Study of an On-ice Air Flow over the Arctic Marginal Sea-ice Zone', *Boundary-Layer Meteorol.* **107**, 189–217.

- Walter, B. A.: 1980, 'Wintertime Observations of Roll Clouds over the Bering Sea', *Mon. Wea. Rev.* **108**, 2024–2031.
- Weckwerth, T. M., Wilson, J. W., Wakimoto, R. M., and Crook, N. A.: 1997, 'Horizontal Convective Rolls: Determining the Environmental Conditions Supporting their Existence and Characteristics', *Mon. Wea. Rev.* **125**, 505–526.